Scientific African 21 (2023) e01763

Contents lists available at ScienceDirect

Scientific African

journal homepage: www.elsevier.com/locate/sciaf

Comparison of multi-source remote sensing data for estimating and mapping above-ground biomass in the West Usambara tropical montane forests

7.1.14

Sami D. Madundo[a,b,*], Ernest W. Mauya[b], Charles J. Kilawe[a]

[a] Department of Ecosystems and Conservation, Sokoine University of Agriculture, College of Forestry Wildlife and Tourism, Tanzania
[b] Department of Forest Engineering and Wood Sciences, Sokoine University of Agriculture, College of Forestry Wildlife and Tourism, Tanzania

ARTICLE INFO

Article history:
Received 6 September 2022
Revised 30 March 2023
Accepted 14 June 2023

Editor: DR B Gyampoh

Keywords:
Above-ground biomass
Montane forests
Optical remote sensing
SAR
GAM
XGBoost

ABSTRACT

Above-ground biomass (AGB) estimation is important to better understand the carbon cycle and improve the efficiency of forest policy and management activities. AGB estimation models, using a combination of field data and remote sensing data, can largely replace traditional survey methods for measuring AGB. There are, however, critical steps for mapping AGB based on satellite data with an acceptable degree of accuracy, such as choice of remote sensing data, the proper statistical modelling method, and remote sensing predictor variables, at known field locations. This study sought to identify the optimal optical and synthetic aperture radar (SAR) remote sensing imagery from five sensors (PlanetScope, Sentinel-2, Landsat 8 OLI, ALOS-2/PALSAR-2, and Sentinel-1) to model 159 field-based AGB values from two montane forests under semiparametric (Generalized Additive Model; GAM) and non-parametric (eXtreme Gradient Boosting; XGB) approaches using information from four groups of predictor variables (spectral bands/polarizations, vegetation indices, textures, and a combination of all). The study's results showed that PlanetScope (rRMSE = 69.19%; R^2 = 0.161) was the most precise optical sensor while ALOS-2/PALSAR-2 (rRMSE = 70.76; R^2 = 0.165) was the most precise amongst the SAR sensors. XGB models generally resulted in those with lower prediction errors as compared to GAMs for the five sensors. Models having textures of vegetation indices and polarization bands achieved greater accuracy than models that incorporated spectral bands/polarizations and vegetation indices only. The study recommends that PlanetScope and ALOS-2/PALSAR-2 remote sensing data using the XGB-based technique is an appropriate approach for accurate local and regional estimation of tropical forest AGB particularly for complex montane forest ecosystems.

Introduction

Above-ground biomass (AGB) is crucial factor for forest ecosystems to carry out their ecological functions and is a vital indicator of the capacity of forests to sequester carbon. The Global Climate Observing System recognizes AGB as a key

* Corresponding author.
E-mail address: sami.madundo@sua.ac.tz (S.D. Madundo).

https://doi.org/10.1016/j.sciaf.2023.e01763

quantity when estimating terrestrial carbon stocks as an essential variable in monitoring climate change [11]. An accurate estimation of AGB could considerably enhance our understanding of the study of carbon cycling and climate changes on a global scale.

Traditionally, AGB has been accurately quantified at a local scale through field-based inventories. However, over larger areas, these inventories become costly and spatially limited, especially in steep, mountainous, and complex terrain [27]. In this context, spatially explicit information on AGB is crucial for estimating carbon sequestered and carbon dioxide exchanged. Utilizing remote sensing data, combined with statistical techniques that are calibrated and validated with field measurements, enables the derivation of spatially representative maps of forest AGB across larger scales [2] and at lower costs [26].

Improvements in remote sensing technologies and open-access policies have resulted into various sources of valuable satellite remote sensing data in estimating forest parameters including AGB. The Sentinel-2 MultiSpectral Instrument (MSI), Landsat 8 Operational Land Imager (OLI), and Sentinel-1 Synthetic Aperture Radar (SAR) imageries offer capabilities for AGB modelling by means of both active and passive remote sensing systems. The Japanese Aerospace Exploration Agency (JAXA) issues global mosaics of Advanced Land Observing Satellite (ALOS) dual-polarised Phased Array type L-Band SAR (PALSAR) backscatter data annually, which have penetrability and pixels that comprise broad information concerning the positioning and assembly of forest canopy and stems. This renders the ALOS/PALSAR global mosaics particularly useful for AGB mapping. Additionally, PlanetScopes' high-resolution (4.77 m) satellite imagery has recently been made public via Norway's International Climate and Forest Initiative (NICFI), Kongsberg Satellite Services (KSAT), along with its associates Planet plus Airbus [50]. PlanetScope data, which covers the tropics only, is meant to advance forest monitoring in these countries in implementing sustainable forest management and REDD+ [42]. Identifying the optimal satellite remote sensing sensors for AGB modelling in such complex areas is of particular importance.

Remote sensing data is a critical element in AGB modelling, but it is not enough on its own. To accurately estimate AGB, three other factors are critical: proper field sample collection (plots of at least 0.25 ha), the selection of appropriate variables, and the use of modelling algorithms [35]. While spectral bands are commonly used in remote sensing-based AGB estimation, studies have shown that the inclusion of vegetation indices and texture variables can significantly improve results, particularly in dense tropical forests [31,46,47]. For example, research by Lu et al., [34] in the Brazilian Amazon found that combining spectral bands and textural characteristics improved AGB estimation, particularly in primary forests with intricate canopy systems. The visible, near-infrared, and shortwave infrared bands are typically the most effective spectral bands for AGB estimation, especially in forests with simple stand structures. (e.g., [31,33]).

While ordinary least-square (OLS) regression is commonly used for modelling forest structure attributes using remotely sensed data due to its ease of implementation and interpretation [45], it is limited in its ability to capture the complex non-linear relationship between AGB and remote sensing variables [63] compared to semi-parametric and non-parametric methods. In highly dense and multi-layer canopy forests, remote sensing data saturation occurs at AGB values between 100 and 150 Mg ha^{-1} indicating a plateauing relationship between AGB and remote sensing information [35]. This saturation problem has led to an increase in the adoption of semi-parametric and non-parametric statistical approaches such as Generalized Additive Models (GAM) and machine learning algorithms like Extreme Gradient Boosting (XGB), which can handle non-linear relationships and provide more accurate AGB estimates [19,61,66]. While these methods have been extensively studied in temperate forests, research on their applicability to tropical forests, especially those in Africa, is limited. As tropical trees have shown decreases in growth and photosynthesis at high temperatures, it is important to explore the sustainability of different modelling approaches in these sensitive ecosystems [40]. Despite significant progress in remote sensing-based biomass estimation over the past three decades, identifying relevant variables from different remote sensing data and developing appropriate estimation models for specific studies remains a challenge.

Previous research has identified a lack of studies comparing the performance of different sources of remote sensing data under semi-parametric and machine learning techniques for predicting AGB [57]. It is crucial to understand how the selection of the modelling approach and data sources affects the precision of AGB predictions [14,51,54]. Furthermore, the selection of data source and modelling technique should be specific to the features of the forests being examined and research objectives [12]. The western block of the Usambara mountains in Tanzania has locally rich biomass forests [41], making it an ideal location to compare various approaches for modelling and mapping biomass from remote sensing bands, vegetation indices, and texture metrics from different remote sensing sensors.

To address this gap, this study evaluated and compared several open-access remote sensing products to determine their ability to provide AGB predictions for tropical montane forest ecosystems. Specifically, this research sought to (i) assess the performance of semi-parametric (GAM) and machine learning (XGB) techniques in modelling and mapping AGB from Landsat 8 OLI, Sentinel-2 MSI, PlanetScope, ALOS/PALSAR Global mosaic, and Sentinel-1 bands, vegetation indices, and texture metrics, (ii) identify the most effective bands/polarizations, vegetation indices and texture metrics for predicting AGB, and (iii) produce wall-to-wall spatial prediction AGB maps using the best satellite data and modelling technique.

Materials and methods

Study area

In this study, biophysical data were gathered from forests of the West Usambara mountains, a sizable upland block in Tanzania's Eastern Arc Mountains (Fig. 1). With more than 50% of moist forests confined to this chain, their high carbon stor-

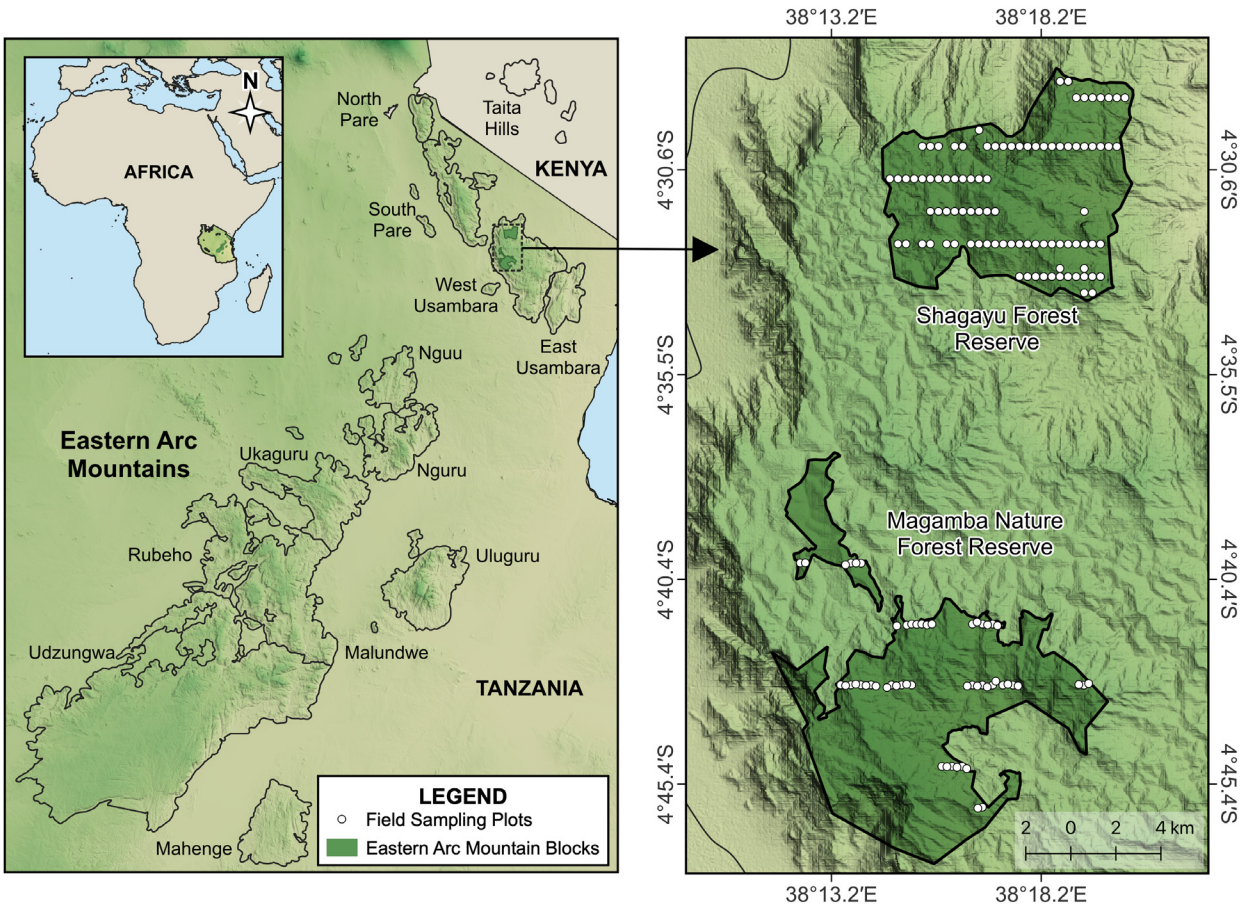

Fig. 1. Location map of the study area.

age potential puts their conservation in a global context. As a result, protocols for monitoring forest above-ground biomass would be beneficial in developing conservation and management strategies for the Eastern Arc Mountains and other relevant forest ecosystems. Covering the entire block was made impossible due to limitations in cost and time resources. Thus, one nature forest reserve and one forest reserve, namely Magamba and Shagayu respectively, were selected for this study. Because of the West Usambara Mountains' proximity to both the equator and the Indian Ocean, their climate is oceanic with bimodal rainfall. Peak rainy months are April and November. The wettest regions experience a maximum annual rainfall of 2000 mm, while rain shadow regions see less than 600 mm of rainfall. The chosen forests are comparatively drier than the other moist forests that can be found on the wetter mountain sides to the east, south, and north.

An overview of the study design

In this remote-sensing supported forest inventory, the potential for AGB estimation from several open access data sources was evaluated. The method can be broken down into four phases: (1) gathering and pre-processing field and remote sensing data, (2) extracting remote sensing variable values from plot locations, (3) selection of optimal variables, and (4) creating predictive models with various variable setups and evaluating their accuracy through cross-validation (Fig. 2). The phases are further explained in the sections that follow.

Data collection

Forest inventory data

A systematic sampling design was undertaken in each forest. A 225 × 900 m grid was created for Magamba Nature Reserve, while a 350 × 700 m grid was used for Shagayu Forest Reserve. Sample plot coordinates were extracted at each grid intersection within the forest. However, due to constraints in terrain and cost, not all plots were recorded, although an effort was made to collect data from plots covering various elevational ranges, which is a key determinant of AGB in mountainous forests. Thus, a total of 159 circular plots were established (Shagayu = 104, Magamba = 55) in March 2020.

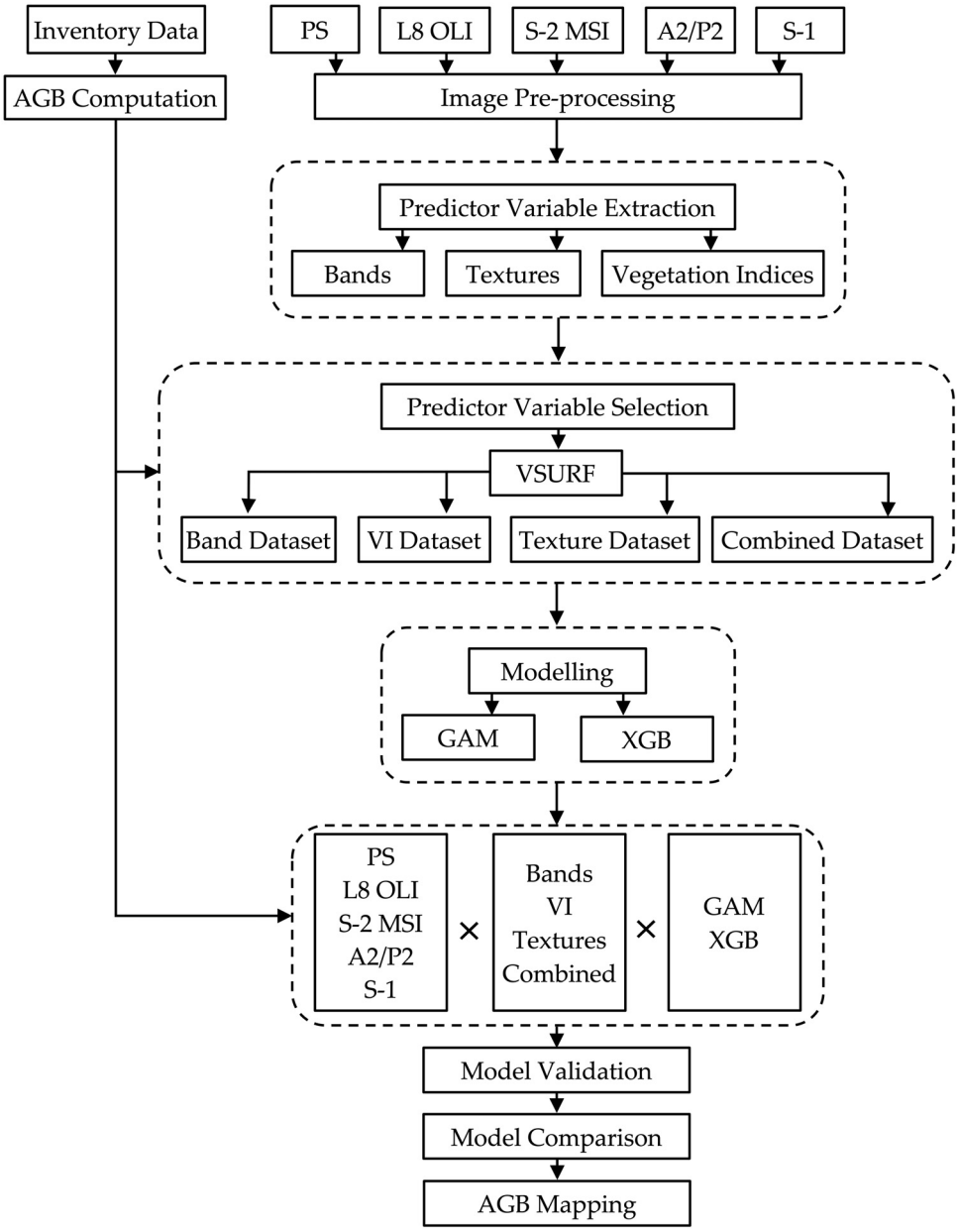

Fig. 2. Methodological framework of estimating AGB using two modelling methods, inventory data and images from PlanetScope (PS), Sentinel-2 (S-2 MSI), Landsat 8 (L8 OLI), ALOS-2/PALSAR-2 (A2/P2), and Sentinel-1 (S-1).

A Garmin N98 was used to locate the sampling units on the ground. Tree height and diameter at breast height (DBH) were measured as biophysical characteristics in each sample plot. The survey did not record any trees having a DBH of less than 5 cm. AGB values for each tree were then computed using an allometric model [39]. The total AGB for each plot was then scaled to a value per hectare based on the corresponding plot area.

Remote sensing data acquisition and pre-processing

Three optical (PlanetScope, Sentinel-2 and Landsat 8) and two SAR (ALOS/PALSAR-2 and Sentinel-1) remote sensing sources were utilized. The remote sensing imagery utilized to estimate the forest AGB for this investigation is summarized in Table 2.

Landsat 8 OLI. A single cloud-free Landsat 8 OLI scene from 4 July 2020, with a Path and Row of 167/063, was retrieved from the USGS GloVis website (https://glovis.usgs.gov). Using the ***RStoolbox*** package (Leutner et al., 2017) in R, the Level-1

Table 1
Statistics of above-ground biomass (Mg ha^{-1}) of the two forests.

Forest	Number of plots	Mean	Minimum	Maximum	Standard deviation
Shagayu	104	334.56	4.33	1289.18	235.30
Magamba	55	225.19	19.05	720.79	174.04
All	159	296.73	4.33	1289.18	221.74

Table 2
Acquired satellite remote sensing data covering Magamba (MG) and Shagayu (SH) forests.

Satellite	Acquisition date	Resolution	Level	Spectra/Polarizations
Landsat 8 OLI	4 July 2019	30 m	L1 TP	B02, B03, B04, B05, B06, B07
Sentinel-2 MSI	12 March 2019 (MG) 16 April 2019 (SH)	10/20 m	L1C	B02, B03, B04, B05, B06, B07, B08, B8A, B11, B12
PlanetScope	December 2019	4.77 m	L1	B, G, R, NIR
ALOS/PALSAR-2	2020	25 m	L1.0	L-band: HH, HV
Sentinel-1	14 March 2020	10 m	L1 GRD	C-band: VV, VH

radiometrically and precision terrain-corrected product (U.S. Geological Survey, 2019) was atmospherically corrected from Top-of-Atmosphere to surface reflectance using the 'radCor' function and finally projected to Arc 1960/UTM zone 37S. The blue (B02), green (B03), red (B04), near-infrared (B05), shortwave infrared-1, SWIR-1 (B06), and SWIR-2 (B07) bands were included while the coastal aerosol, panchromatic, and thermal infrared bands were not.

Sentinel-2 MSI. Sentinel-2 MSI radiometrically corrected Level 1C data were acquired on 12 March 2019 and 16 April 2019 (Table 1) from the Copernicus Open Access Hub (https://scihub.copernicus.eu/dhus/#/home). The multispectral bands with a spatial resolution of 10 m used were; Band 2 (B02) Blue, B03 (Green), B04 (Red), and B08 (Near-Infrared, NIR). The 20 m spatial resolution bands used were B05 (Red-edge 1), B06 (Red-edge 2), B07 (Red-edge 3), B8A (Narrow NIR), B11 (Shortwave infrared, SWIR 1), and B12 (SWIR 2). Using the ***sen2r*** package [53], the Level 1C top of the atmosphere (TOA) reflectance data were subsequently processed to Level 2A via the European Space Agency's (ESA) Sen2Cor algorithm [32] to acquire bottom of the atmosphere (BOA) reflectance images. To ensure spatial coherence, the 20 m bands were resampled to 10 m resolution. The study region required two images; thus, mosaicking was used to combine the images before reprojection.

PlanetScope basemaps. The NICFI distributed imagery, available at https://www.planet.com/basemaps/, are basemaps (mosaics) covering the tropics with a spatial resolution of 4.77 m. These analysis-ready datasets have four spectral bands (Red, Blue, Green, and Near-infrared) [50]. The products are released on a biannual and monthly basis from a temporal perspective, and for this investigation, tiles from the monthly December 2019 product were used. The only processing performed on the PlanetScope imagery was mosaicking and reprojection.

ALOS-2/PALSAR-2 global mosaic. Global 25 m resolution ALOS-2/PALSAR−2 annual mosaic of the year 2020, which is freely available at https://www.eorc.jaxa.jp/ALOS/en/palsar_fnf/fnf_index.htm, was acquired. The Japanese Aerospace Exploration Agency (JAXA) pre-processes this dual polarization (HH and HV) dataset using L-band SAR imagery of the backscattering coefficient obtained by the Advanced Land Observing Satellite-2 (ALOS-2). The mosaic is made up of $10 \times 10^{\circ}$ tiles that have been pre-processed to remove topographic effects and adjusted for geometric errors [58]. The mosaic tiles were calibrated to γ^0 using the following equation:

$$\gamma^0 = 10 \times \log_{10}(\mathrm{DN})^2 + \mathrm{CF} \quad (1)$$

where γ^0 is the gamma-naught in decibels (dB), DN is the digital number in unsigned 16 bits, and CF is a calibration constant of 83.0 dB. Reprojection and image clipping were then performed on the images in R.

Sentinel-1. Amongst the SAR data used in this study, was a single Ground Range Detected (GRD) product acquired from the Sentinel-1A satellite, which is a C-band SAR with a central frequency of 5.405 GHz [38]. The level-1 product with two polarizations was acquired on 14 March 2020 and downloaded from the Copernicus Open Access Hub. The GRD data were pre-processed using the Sentinel Application Platform (SNAP) to obtain the dual-polarised (VV, VH) gamma-naught backscatter values. The pre-processing steps included (1) thermal noise removal, (2) calibration, (3) Lee sigma speckle filtering, (4) range doppler terrain correction, and (5) conversion to γ^0 dB [13]. Subsequent pre-processing (reprojection and image clipping) was carried out in R.

Vegetation indices and texture metrics

The atmospherically corrected images from each sensor were then used to create selected vegetation indices (Table 3) and textures (Table 4) in R. The study included five broadband optical vegetation indices (Normalized Difference Vegetation Index, Difference Vegetation Index, Ratio Vegetation Index, Green Normalized Vegetation Index, and Enhanced Vegetation

Table 3
Description of vegetation indices used as candidate independent variables for AGB modelling.

Index	Name	Expression	Sensor	Reference
DVI	Difference Vegetation Index	NIR-Red	L8, S-2, PS	Richardson & Wiegand [55]
EVI	Enhanced Vegetation Index	2.5[(NIR-Red)/(NIR+2.4Red + 1)]	L8, S-2, PS	Liu & Huete [23]
GNDVI	Green Normalized Difference Vegetation Index	(NIR - Green)/(NIR + Green)	L8, S-2, PS	Gitelson et al. [17]
NDVI	Normalized Difference Vegetation Index	(NIR - Red)/(NIR + Red)	L8, S-2, PS	Rouse et al. [56]
RVI	Ratio Vegetation Index	NIR/Red	L8, S-2, PS	Pearson & Milton [48]
CLRE	Chlorophyll Red-Edge	(RE3/RE1) - 1	S-2	Gitelson et al. [16]
ND-RE1	Normalized Difference Red Edge	(RE2 – RE1)/(RE2 + RE1)	S-2	Gitelson & Merzlyak [18]
ND-RE2	Normalized Difference Red Edge	(RE3 – RE1)/(RE3 + RE1)	S-2	Barnes et al. [1]
CPR	Cross-polarized Ratio	HV/HH VH/VV	A2/P2 S-1	Omar et al. [45]
DpRVI	Dual-polarized Radar Vegetation Index	4HH/(HH+HV) 4VV/(VV+VH)	A2/P2 S-1	Holtgrave et al. [21]
RFDI	Radar Forest Degradation Index	(HH-HV)/(HH+HV) (VV-VH)/(VV+VH)	A2/P2 S-1	Nicolau et al. [44]

Table 4
General description of grey-level co-occurrence matrix (GLCM) texture metrics used in this study.

Texture	Expression	Expression
Mean (**mea**)	$\mu_i = \sum_{i,j=0}^{N-1} iP_{i,j}$	Mean of grey level (GL) distribution of the image.
Variance (**var**)	$\sum_{i,j=0}^{N-1} iP_{i,j}(i-\mu_i)^2$	GLCM variance is a measure of the dispersion of GL distribution
Contrast (**con**)	$\sum_{i,j=0}^{N-1} iP_{ij}(i-j)^2$	Contrast indicates the amount of local GL variation in an image. Large values indicate the presence of edges, noise or wrinkled features.

Source: Haralick et al., [20].

Index) as well as three narrowband indices specific to Sentinel-2 (Normalized Difference Red Edge 1, Normalized Difference Red Edge 2 and Chlorophyll Red-Edge). The Sentinel-2 narrowband indices were utilized to assess their AGB modelling capability. Furthermore, three indices for the SAR sensors were computed, these were the Cross-polarized ratio, Dual-polarized Radar Vegetation Index, and the Radar Forest Degradation Index. Texture metrics were computed using a 3 × 3 window for each of the sensors' bands and vegetation indices.

Predictor variable selection

Depending on the satellite sensor, the total pre-selected predictors of bands, indices, and texture variables ranged from 20 to 54. Variable selection was first carried out to ensure that robust models were created for the various datasets and predictor variables [36]. The R package ***VSURF*** was applied to the original bands/polarizations, indices, and texture datasets to determine the appropriate predictors. Random forests are used as the primary classifier in ***VSURFs*** wrapper-based technique [15]. To decrease the number of features and increase model accuracy, predictor variables are first rated according to a variable importance measure. Low-scoring predictors are then discarded. A ranked list of only the most significant predictors is created in the last phase.

Statistical modelling approaches

Semi-parametric and non-parametric statistical modelling approaches were used for estimating AGB. The details for each approach are given below.

Generalized additive models

A generalized additive model (GAM) is based on piecewise polynomials, which describe the contribution of each predictor variable. These polynomials are merged into an independent function (Eq. (2)) that is bounded by a smoothing spline. In this study, GAMs were fitted for each satellite sensor using a Gaussian error distribution and a logarithmic link function to relate the plot level AGB. This model form was preferred as it offers acceptable estimates when true zeros are present in the estimate of AGB, which has continuous positive values. The R package ***mgcv*** [68] was used to carry out the GAM regression. Each predictor variable that entered the model received a smoothing spline with a smoothing parameter, k, of 3.

$$ln(y_i) = b_0 - \sum_{i=1}^{n} f_i(x_i) \quad (2)$$

where, y_i is the ground reference AGB (Mg ha^{-1}) b_0 is a constant term (the intercept); $f_i(x_i)(i = 1, 2,\ldots,n)$ is a smoothing function for each independent variable.

Extreme gradient boosting

XGB is a boosting algorithm that is based on gradient boosting decision trees and random forest methods. In very large-scale data training, it is a versatile and highly scalable tree structure enhancement model that can handle sparse data, significantly increase algorithm performance, and decrease computational memory. The R package ***xgboost*** [4] was used to implement the XGB.

Statistical measures for evaluation of model performance

The accuracy of the models was evaluated using k-fold cross validation, where $k = 10$ (each model was re-fit 10 times using 90% of the data, and predictions from the fitted models were compared with observations of the remaining 10% of the data). The relative root-mean-square error (rRMSE) and coefficient of determination (R^2) were used to assess the model's performance. A higher R^2 score and a lower rRMSE value typically signify a model's ability to estimate information more precisely.

$$RMSE = \sqrt{\sum_{i=1}^{n} \frac{(\widehat{y_i} - y_i)}{n}} \tag{3}$$

$$rRMSE = \frac{RMSE}{\bar{y}} \times 100 \tag{4}$$

$$R^2 = 1 - \frac{\sum_{i=1}^{n} (y_i - \widehat{y_i})^2}{\sum_{i=1}^{n} (y_i - \overline{y_i})^2} \tag{5}$$

AGB maps

Finally, the best performing optical and SAR data were used to create spatial prediction maps of the study sites AGB using the R ***raster*** package [10].

Results

Model performance

A total of 40 models were developed, 20 for both the semiparametric (GAM) and non-parametric (XGB) techniques. Predictors selected during variable selection were used in both modelling techniques, with the minimum number of predictors being two in a model to a maximum of eight (Table 5). The values for R^2 and rRMSE across the five datasets using GAM ranged from 0.051 to 0.152 and 71.23–74.02% respectively. Additionally, the values for R^2 and rRMSE across the five datasets using XGB ranged from 0.051 to 0.199 and 69.19–77.67% respectively. Based on the lowest rRMSE, the best model amongst the optical sensors was that of PlanetScope using combined predictors (rRMSE = 69.19%) while the best model amongst the SAR sensors came from ALOS-2/PALSAR-2 using texture variables (rRMSE = 70.76%). Both models were modelled under XGB techniques.

Predictor variable selection

For each remote sensing dataset, four categories of predictor variables were prepared. These categories consisted of the native bands or polarizations of the sensor (B), derived vegetation indices (VI), textures of the bands/polarizations and vegetation indices (T), and a combination of the sensors bands/polarizations, vegetation indices and textures (C). For the PlanetScope model, variable selection under VSURF returned predictors from the combined category. The selected PlanetScope predictors were contrast of EVI (pEVI.con), GNDVI (pGNDVI), and variance of RVI (pRVI.mea) (Fig. 3). Texture variables were found to be the most significant predictor variables for the ALOS-2/PALSAR-2 model, particularly variance of HH and HV, and the mean of HV.

Estimation and mapping of AGB using selected models

For the chosen XGB models and remote sensing data, Table 6 displays the estimated mean AGB, 95% confidence interval (CI), and standard deviation of the mean AGB estimates. The predictions from the ALOS-2/PALSAR-2 and PlanetScope models returned mean AGB estimates of 298.16 Mg ha^{-1} and 276.20 Mg ha^{-1} respectively. For both models, the spatially predicted estimates of the mean AGB were within 95% confidence intervals of the mean AGB based solely on the field data (that is,

Table 5
Performance of GAMs and XGB models fitted with predictors from the five satellite sensors. Bold text indicates best perfoming models with lowest rRMSE.

Sensor	Satellite	Category	Predictors	GAM		XGB	
				rRMSE	R^2	rRMSE	R^2
Optical	PS	Bands	pB, pG, pNIR, pR	72.86	0.067	74.05	0.051
		Indices	pRVI, pGNDVI	71.43	0.069	73.74	0.113
		Textures	pEVI.con, pRVI.mea, pNDVI.con	72.06	0.075	69.56	0.148
		Combined	pEVI.con, pGNDVI, pRVI.mea	71.85	0.083	**69.19**	**0.161**
	S-2	Bands	msiB05, msiB03, msiB06, msiB11	72.55	0.079	71.25	0.137
		Indices	msiNDRE2, msiEVI	73.43	0.051	73.98	0.076
		Textures	msiB05.var, msiB04.con, msiNDVI.con, msiB12.var, msiB02.con	73.22	0.087	71.32	0.116
		Combined	msiB05, msiB05.var, msiB04.con, msiB11, msiNDVI.con	72.02	0.077	70.45	0.146
	L8 OLI	Bands	oliB03, oliB07, oliB06, oliB04, oliB02	73.35	0.083	75.23	0.055
		Indices	oliNDVI, oliGNDVI	72.42	0.059	72.17	0.101
		Textures	oliEVI.con, oliRVI.con, oliEVI.mea, oliGNDVI.con	72.30	0.112	70.19	0.199
		Combined	oliRVI.con, oliNDVI.con, oliEVI.con, oliRVI, oliGNDVI, oliGNDVI.con	72.14	0.152	70.76	0.187
SAR	A-2/P-2	Polarizations	aHH, aHV	72.24	0.053	74.48	0.068
		Indices	aCPR, aDpRVI, aRFDI	71.40	0.075	73.33	0.076
		Textures	aHH.var, aHV.var, aHV.mea	71.23	0.099	**70.76**	**0.165**
		Combined	aHH.var, aHV.var, aHV.mea, aHH, aHV, aCPR, aDpRVI, aRFDI	71.53	0.110	73.16	0.085
	S-1	Polarizations	sVV, sVH	74.02	0.070	77.01	0.073
		Indices	sCPR, sDpRVI, sRFDI	72.91	0.051	77.32	0.073
		Textures	sVV.mea, sVH.var, sVV.var, sCPR.mea, sVH.con, sVV.con	73.91	0.065	76.84	0.074
		Combined	sVV.mea, sVH.mea, sVV.var, sVV, sCPR.var, sVV.con	72.47	0.090	77.67	0.072

Table 6
Estimated mean AGB (Mg ha^{-1}), lower and upper 95% confidence intervals (CI) for the mean AGB estimates in Mg ha^{-1}, and standard deviation (SD) of the mean estimates (Mg ha^{-1}) for the selected models.

Data	Mean	Lower limit 95% CI	Upper limit 95% CI	SD
Inventory	296.73	262.62	331.19	221.74
ALOS-2/PALSAR-2	298.16	285.28	311.05	97.03
PlanetScope	276.20	263.71	288.69	97.08

262.62–331.19 Mg ha^{-1}). In contrast to the estimate from the PlanetScope model, the estimated mean AGB of the ALOS-2/PALSAR-2 model was closer to the field-estimated mean AGB (i.e., 296.73 Mg ha^{-1}). Additionally, the AGB estimations based on both models had a higher precision than the field estimate.

AGB maps of the forests using the best models are presented in Fig. 4. Visual inspection of the spatially predicted AGB via the two models shows that, the AGB distribution across the landscape agrees very well with a what is seen through the false-colour composite of the PlanetScope scene. In plots where the observed AGB was extremely low or close to zero, the two models tended to overestimate AGB. Furthermore, for plots with exceptionally high biomass values, the models tended to underestimate AGB (Fig. 5).

Discussion

Accurate and timely estimation of forest biomass using remotely sensed data is critical for suitable for sustainable forest management and understanding the global carbon cycle. However, several factors affect the accuracy of AGB estimation using remote sensing predictors, including the choice of remote sensing data, modelling methods, and predictor variables. This study aimed to address these key factors using field data obtained from tropical montane forests of Tanzania to develop better approaches for remotely sensed-assisted forest inventories.

Predictive performance of modelling methods

In this study two modelling techniques were used to estimate forest AGB, and the non-parametric approach was found to perform the best. However, the accuracy of the estimates obtained from these approaches can be influenced by factors

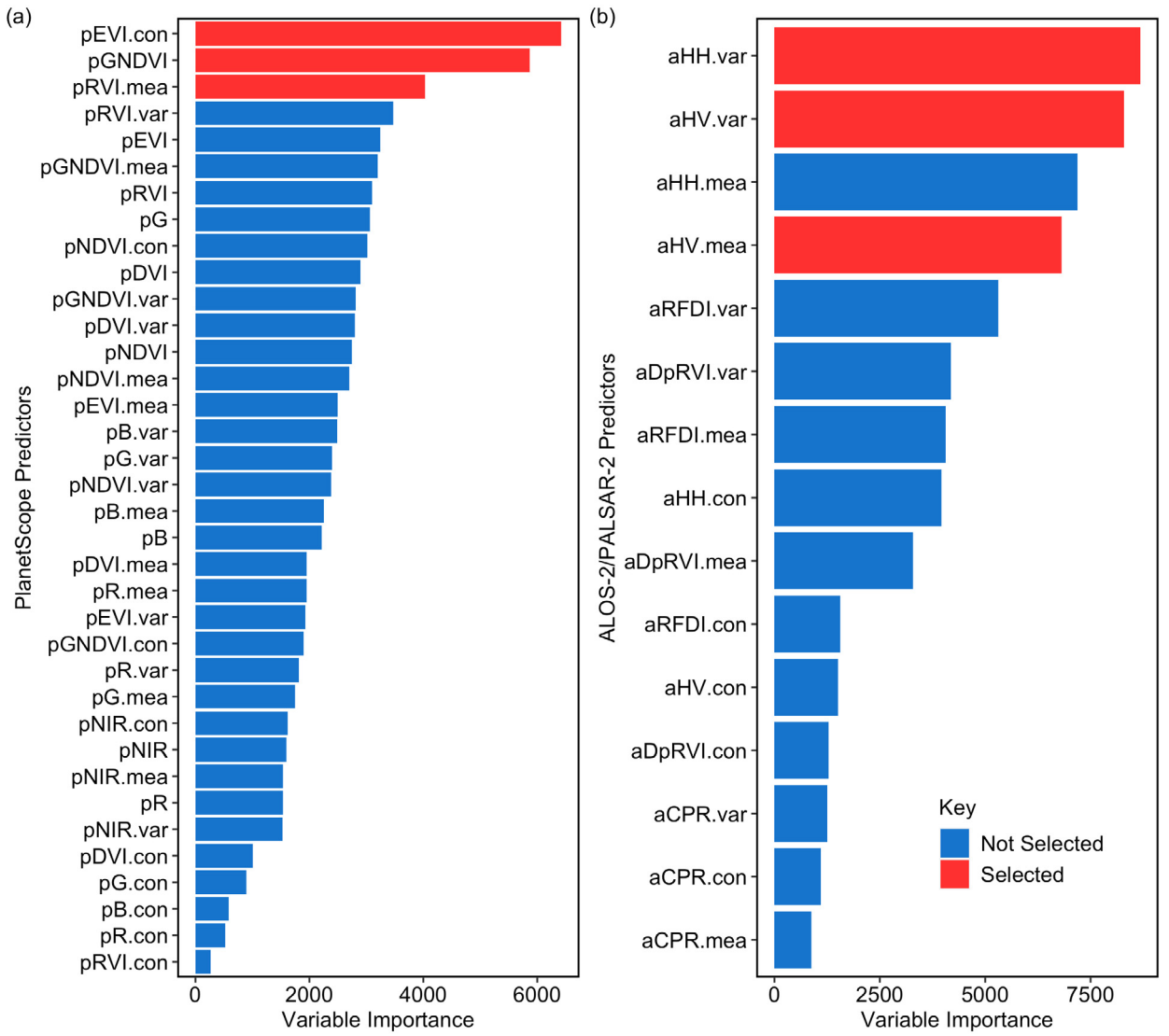

Fig. 3. Important predictor variables for the optimal remote sensing data sets.

such as the forest's characteristics, inventory sample size, remote sensing data used, and technique of accuracy evaluation. To evaluate the effect of remote sensing data and validation metrics on remote sensing-based AGB prediction, we used two distinct modelling approaches in this study.

Although the difference in performance between the two modelling techniques used in this study was marginal, it is consistent with findings from other investigations. For instance, Li et al., [28] reported that XGB outperformed random forest (RF), and Li et al. [30], found that XGB performed better than two other algorithms including random forest and linear regression. Similarly, Pham et al. [49] reported that a hybrid XGB with genetic algorithm (XGB-GA) performed best of four machine-learning algorithms assessed for AGB prediction. On the other hand, in some studies, such as those by Halperin et al. [19], Moisen & Frescino [43], or Soriano-Luna et al. [61], GAM was found to outperform other modelling techniques, including linear regression and random forest. These results suggest that the selection of the most suitable modelling method appears to be specific to the characteristics of the dataset of a particular area of study.

Ideal optical and SAR remote sensing data sets

Our study highlights the potential of optical or SAR-based biomass estimates for enhancing AGB mapping and supporting decision-making. amongst the optical models tested, the PlanetScope model contributed the most to improving the accuracy of AGB estimates. Compared to Sentinel-2 and Landsat 8 OLI, PlanetScope's higher spatial resolution may have enabled a better separation of tree species with varying canopy greenness [62] as accounted for by the contribution of GNDVI in the

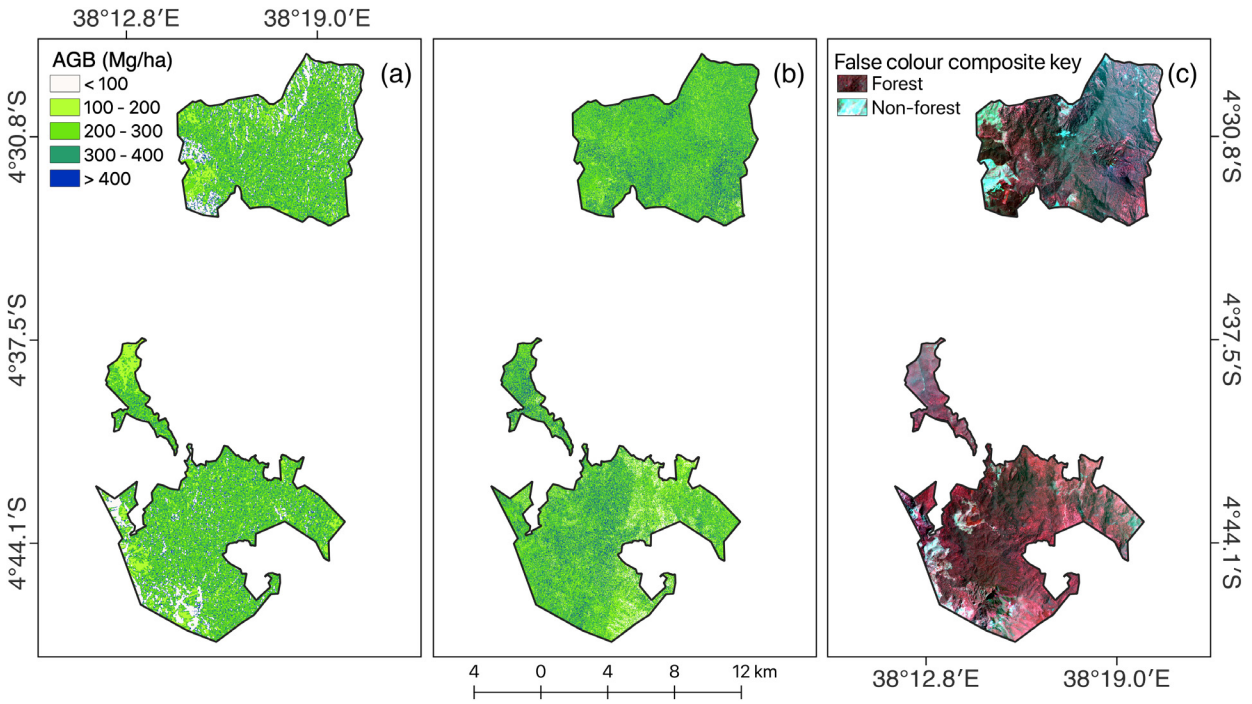

Fig. 4. Spatial distribution of AGB using XGB models of (a) ALOS-2/PALSAR-2 and (b) PlanetScope, while (c) is a false colour composite (NIR-R-G in the RGB channels) of the PlanetScope image.

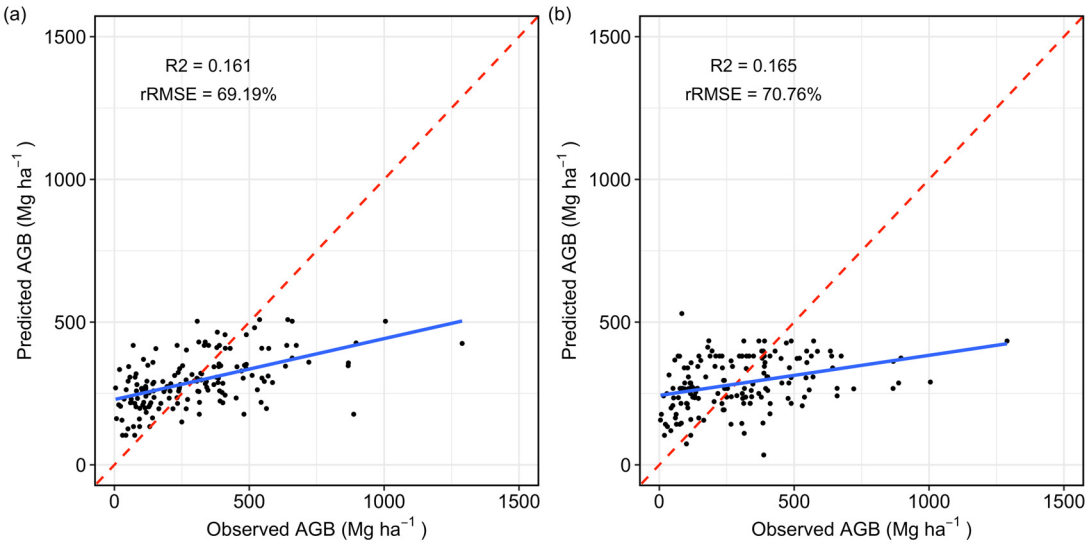

Fig. 5. Observed versus model predictions data for plot level AGB resulting from XGB models of (a) ALOS-2/PALSAR-2 and (b) PlanetScope for the forests. Dotted lines represent the 1:1 line and solid lines represent the slope.

model. Additionally, high-resolution textures derived from PlanetScope imagery provided a more detailed representation of vegetation structural components [60], which led to the greater model precision achieved. These findings align with previous studies which reported similar performance of PlanetScope imagery in estimating forest AGB [5] and other vegetation properties; such as pasture canopy height [8].

For SAR data, our analysis revealed that ALOS-2/PALSAR-2 imagery outperformed Sentinel-1 in terms of AGB estimation accuracy. This finding is consistent with previous studies that have shown that longer SAR sensors wavelength (such as the L- and P-bands) to be more strongly correlated with forest biomass, with HV-polarized backscatter coefficients being more

sensitive to biophysical forest charateristics than C-band and co-polarization bands [59,65]. The variable importance results presented in Fig. 3(b) also support the inclusion of HV backscatter coefficients' in the ALOS-2/PALSAR-2 prediction model.

Important remote sensing predictor variables

Accurately estimating AGB from remote sensing data requires a thorough understanding of the relationship between AGB and various spectral and polarization information. In this study, we utilized a wide range of SAR and spectral data, including raw bands/polarizations, band/polarization ratios, vegetation indices, and textures. Previous studies by Li et al. [29] and Purnamasari et al. [52] have demonstrated that these types of data are effective for remote sensing-based biomass estimations. Our results show that the best explanatory variables can be chosen from a specified set of variables or groups of variables. amongst the explanatory variables we examined in this study, we found that mean and variance texture metrics of vegetation indices (for PlanetScope data) and raw polarizations (for ALOS-2/PALSAR-2 data) were the most effective predictors for producing precise AGB models. The mean texture measure smooths the image and reduces background interference by averaging the values of the grey tones. On the other hand, the variance texture measure is directly related to the high fluctuations in grey tone values, mostly brought on by variances in the forms of leaves across the forest. The texture values in an image enable the evaluation of the spatial variability in the various plant types, which exhibit distinctive phenological patterns connected to structure, development stage, carbon exchange, and vegetative greenness [25,67].

The GLCM-based textures can reflect the differences in interconnected traits of tree species such as leaf shape, colour, angle, size, and density [8]. Textural measurements can help AGB models make more accurate predictions if the right processing methods are employed [47]. Compared to spectral reflectance or band ratios, textures are more effective at capturing the diverse forest canopy structures of the forest strata due to their sensitivity to the spatial characteristics of the canopy shadow [9]. Thapa et al. [64] utilized SAR imagery acquired from the ALOS PALSAR satellite and texture images to estimate the above-ground carbon stock in Indonesia by multiple linear regression, and they found reduced RMSE values in comparison to the current study. By only using SAR imagery, the authors achieved a regression RMSE of 45.64 Mg C ha^{-1}. However, after including the texture variables, the models improved and showed an RMSE between 28.01 and 37.70 Mg C ha^{-1}. Additionally, SAR image textures greatly enhanced biomass mapping using Landsat TM data, according to Cutler et al., [7] and Huang et al., [22]. Our results support the findings of these studies, indicating that texture metrics of remote sensing data are valuable predictors for estimating AGB.

AGB spatial maps of the forests

The per-pixel agreement between the AGB maps created from PlanetScope and ALOS-2/PALSAR-2 data was fair, except in areas where the PlanetScope map had low AGB values. However, when considering the mean AGB for the forests, the prediction from the ALOS-2/PALSAR-2 map appeared to be consistent with the field estimates. Nonetheless, there were several reasons for the discrepancy between the two maps, with the models' inherent limitations being a significant factor. Both the ALOS-2/PALSAR-2 and PlanetScope AGB models overestimated AGB in areas with low field values and underestimate AGB in areas with high measured AGB (Fig. 5), which is in line with previous research findings [3,26,37] and may be due to the models' inability to represent the differentiation in forest structure that occurs within the forest.

The underprediction of AGB in the ALOS-2/PALSAR-2 map could be attributed to the SAR signal becoming saturated at high AGB values. SAR saturation has been identified in several previous studies, with the X- or C-band usually being associated with saturation at significantly lower values than other bands. Similarly, using optical data has been known to overestimate biomass, as reported in several optical data types [24,31].

Overall, the study's results were encouraging, with optimal optical and SAR remote sensing data, modelling techniques, and predictor variables identified for AGB estimation. The selected models produced reasonable improvements in AGB estimation based on the identified variables, which were supported by additional research findings (e.g. [6,28,37]). The study's outcomes revealed that PlanetScope and ALOS-2/PALSAR-2 imagery had reasonable spectral/microwave and spatial features for AGB estimation. These findings could support Tanzania's national REDD+ program's current need for a forest carbon stock estimate. Improved forest data from publicly accessible data sources such as PlanetScope and ALOS-2/PALSAR-2 could support results-based incentives for those who responsibly manage their forest resources responsibly according to accepted standards such as the REDD+ initiatives.

Conclusion

This study is not the first to estimate forest above-ground biomass using PlanetScope, Sentinel, Landsat, and PALSAR data as well as the eXtreme Gradient Boosting technique. It is the first one, though, to compare the predictive power of these open-access remote sensing data to precisely estimate above-ground biomass in part of Tanzania's Eastern Arc montane forests. Continuous monitoring is required to determine their role in the global carbon cycle, including whether they are serving as sources or sinks. The accuracy of estimates was increased by using remote sensing data for AGB estimation. Therefore, by increasing precision, the remote sensing-based methodologies used in this study will complement the field-based estimates of AGB. The models used in this study's AGB estimation, however, showed saturation challenges. Future

research should therefore concentrate on improving these restrictions by employing the synergy of various data sources to increase the estimation efficiency of AGB models beyond what was achieved in the current work.

Declaration of Competing Interest

The authors declare that they have no known competing financial interests or personal relationships that could have appeared to influence the work reported in this paper.

Acknowledgments

The authors acknowledge the financial support received from "The Eastern Arc Mountains Conservation Endowment Fund", which facilitated the completion of this study.

References

[1] E.M. Barnes, T.R. Clarke, S.E. Richards, P.D. Colaizzi, J. Haberland, M. Kostrzewski, P. Waller, C. Choi, E. R, T. Thompson, R.J. Lascano, H. Li, M.S Moran, Coincident detection of crop water stress, nitrogen status and canopy density using ground based multispectral data, Proc. 5th Int. Conf. Precis. Agric. (2000).
[2] P. Bispo, C. da, P. Rodríguez-Veiga, B. Zimbres, S. do Couto de Miranda, C. Henrique Giusti Cezare, S. Fleming, F. Baldacchino, V. Louis, D. Rains, M. Garcia, F. Del Bon Espírito-Santo, I. Roitman, A.M. Pacheco-Pascagaza, Y. Gou, J. Roberts, K. Barrett, L.G. Ferreira, J.Z. Shimbo, A. Alencar, H. Balzter, Woody aboveground biomass mapping of the Brazilian savanna with a multi-sensor and machine learning approach, Rem. Sens. (Basel) 12 (17) (2020) 2685, doi:10.3390/rs12172685.
[3] J.M.B. Carreiras, M.J. Vasconcelos, R.M. Lucas, Understanding the relationship between aboveground biomass and ALOS PALSAR data in the forests of Guinea-Bissau (West Africa), Remote Sens. Environ. 121 (2012) 426–442, doi:10.1016/j.rse.2012.02.012.
[4] T. Chen, C. Guestrin, XGBoost, in: Proceedings of the 22nd ACM SIGKDD International Conference on Knowledge Discovery and Data Mining, 2016, pp. 785–794, doi:10.1145/2939672.2939785.
[5] O. Csillik, P. Kumar, G.P. Asner, Challenges in estimating tropical forest canopy height from planet dove imagery, Rem. Sens. (Basel) 12 (7) (2020) 1–18, doi:10.3390/rs12071160.
[6] O. Csillik, P. Kumar, J. Mascaro, T. O'Shea, G.P Asner, Monitoring tropical forest carbon stocks and emissions using Planet satellite data, Sci. Rep. 9 (1) (2019) 1–12, doi:10.1038/s41598-019-54386-6.
[7] M.E.J. Cutler, D.S. Boyd, G.M. Foody, A. Vetrivel, Estimating tropical forest biomass with a combination of SAR image texture and Landsat TM data: an assessment of predictions between regions, ISPRS J. Photogramm. Remote Sens. 70 (2012) 66–77, doi:10.1016/j.isprsjprs.2012.03.011.
[8] A.A. Dos Reis, J.P.S. Werner, B.C. Silva, G.K.D.A. Figueiredo, J.F.G. Antunes, J.C.D.M. Esquerdo, A.C. Coutinho, R.A.C. Lamparelli, J.V. Rocha, P.S.G Magalhães, Monitoring pasture aboveground biomass and canopy height in an integrated crop-livestock system using textural information from planetscope imagery, Rem. Sens. (Basel) 12 (16) (2020) 1–21, doi:10.3390/RS12162534.
[9] S. Eckert, Improved forest biomass and carbon estimations using texture measures from worldView-2 satellite data, Remote Sens. (Basel) 4 (4) (2012) 810–829, doi:10.3390/rs4040810.
[10] Etten, J.Van, Sumner, M., Cheng, J., Baston, D., Bevan, A., Bivand, R., Busetto, L., Canty, M., Fasoli, B., Forrest, D., Gray, J., Greenberg, J.A., Hiemstra, P., Karney, C., & Mattiuzzi, M. (2015). Package "raster." *R Packgage Version 3.5-21*, 734.
[11] J.-L. Fellous, Towards a global climate observing system, Interdiscipl. Sci. Rev. 33 (1) (2008) 83–94, doi:10.1179/030801808X259952.
[12] Y. Feng, D. Lu, Q. Chen, M. Keller, E. Moran, M.N. Dos-Santos, E.L. Bolfe, M. Batistella, Examining effective use of data sources and modeling algorithms for improving biomass estimation in a moist tropical forest of the Brazilian Amazon, Int. J. Digital Earth 10 (10) (2017) 996–1016, doi:10.1080/17538947.2017.1301581.
[13] F. Filipponi, Sentinel-1 GRD preprocessing workflow, in: Proceedings, 18, 2019, p. 11, doi:10.3390/ecrs-3-06201.
[14] Y. Gao, D. Lu, G. Li, G. Wang, Q. Chen, L. Liu, D. Li, Comparative analysis of modeling algorithms for forest aboveground biomass estimation in a subtropical region, Remote Sens. (Basel) 10 (4) (2018), doi:10.3390/rs10040627.
[15] R. Genuer, J. Poggi, C. Tuleau-malot, R. Genuer, J. Poggi, C.T. Vsurf, A.R. Package, R. Genuer, J. Poggi, C. Tuleau-malot, VSURF : an R package for variable selection using random forests, R J. 7 (2) (2015) 19–33.
[16] A.A. Gitelson, Y. Gritz, M.N Merzlyak, Relationships between leaf chlorophyll content and spectral reflectance and algorithms for non-destructive chlorophyll assessment in higher plant leaves, J. Plant Physiol. 160 (3) (2003) 271–282, doi:10.1078/0176-1617-00887.
[17] A.A. Gitelson, Y.J. Kaufman, M.N. Merzlyak, Use of a green channel in remote sensing of global vegetation from EOS- MODIS, Remote Sens. Environ. 58 (1996) 289–298.
[18] A. Gitelson, M.N. Merzlyak, Spectral reflectance changes associated with autumn senescence of aesculus hippocastanum L. and Acer platanoides L. Leaves. Spectral features and relation to chlorophyll estimation, J. Plant Physiol. 143 (3) (1994) 286–292, doi:10.1016/S0176-1617(11)81633-0.
[19] J. Halperin, V. LeMay, E. Chidumayo, L. Verchot, P. Marshall, Model-based estimation of above-ground biomass in the miombo ecoregion of Zambia, For. Ecosyst. 3 (1) (2016) 1–17, doi:10.1186/s40663-016-0077-4.
[20] R.M. Haralick, K. Shanmugam, I. Dinstein, Textural features for image classification, *IEEE Trans. Syst., Man, Cybernet., SMC-3* (6) (1973) 610–621, doi:10.1109/TSMC.1973.4309314.
[21] A.-K. Holtgrave, N. Röder, A. Ackermann, S. Erasmi, B. Kleinschmit, Comparing sentinel-1 and -2 data and indices for agricultural land use monitoring, Remote Sens. (Basel) 12 (18) (2020) 2919, doi:10.3390/rs12182919.
[22] H. Huang, C. Liu, X. Wang, X. Zhou, P. Gong, Integration of multi-resource remotely sensed data and allometric models for forest aboveground biomass estimation in China, Remote Sens. Environ. 221 (August 2017) (2019) 225–234, doi:10.1016/j.rse.2018.11.017.
[23] Hui Qing Liu, A Huete, A feedback based modification of the NDVI to minimize canopy background and atmospheric noise, IEEE Trans. Geosci. Remote Sens. 33 (2) (1995) 457–465, doi:10.1109/36.377946.
[24] A.B. Imran, K. Khan, N. Ali, N. Ahmad, A. Ali, K. Shah, Narrow band based and broadband derived vegetation indices using Sentinel-2 Imagery to estimate vegetation biomass, Glob. J. Environ. Sci. Manag. 6 (1) (2020) 97–108, doi:10.22034/gjesm.2020.01.08.
[25] K.C. Kelsey, J.C. Neff, Estimates of aboveground biomass from texture analysis of landsat imagery, Remote Sens. (Basel) 6 (7) (2014) 6407–6422, doi:10.3390/rs6076407.
[26] A. Kumar, B.S.P.C. Kishore, P. Saikia, J. Deka, S. Bharali, L.B. Singha, O.P. Tripathi, M.L. Khan, Tree diversity assessment and above ground forests biomass estimation using SAR remote sensing: a case study of higher altitude vegetation of North-East Himalayas, India, Phys. Chem. Earth 111 (March) (2019) 53–64, doi:10.1016/j.pce.2019.03.007.
[27] H. Latifi, M. Heurich, Multi-scale remote sensing-assisted forest inventory: a glimpse of the state-of-the-art and future prospects, Remote Sens. (Basel) 11 (11) (2019) 1260, doi:10.3390/rs11111260.

[28] C. Li, L. Zhou, W. Xu, Estimating aboveground biomass using sentinel-2 msi data and ensemble algorithms for grassland in the shengjin lake wetland, China, Remote Sens. (Basel) 13 (8) (2021), doi:10.3390/rs13081595.
[29] H. Li, T. Kato, M. Hayashi, L. Wu, Estimation of forest aboveground biomass of two major conifers in ibaraki prefecture, Japan, from PALSAR-2 and sentinel-2 data, Remote Sens. (Basel) 14 (3) (2022) 468, doi:10.3390/rs14030468.
[30] Y. Li, M. Li, C. Li, Z. Liu, Forest aboveground biomass estimation using Landsat 8 and Sentinel-1A data with machine learning algorithms, Sci. Rep. 10 (1) (2020) 1–12, doi:10.1038/s41598-020-67024-3.
[31] P.M. López-Serrano, J.L.C. Domínguez, J.J. Corral-Rivas, E. Jiménez, C.A. López-Sánchez, D.J. Vega-Nieva, Modeling of aboveground biomass with landsat 8 OLI and machine learning in temperate forests, Forests 11 (1) (2020) 1–18, doi:10.3390/f11010011.
[32] J. Louis, V. Debaecker, B. Pflug, M. Main-Knorn, J. Bieniarz, U. Mueller-Wilm, E. Cadau, F. Gascon, Sentinel-2 SEN2COR: L2A processor for users, *Eur. Space Agency, (Spec. Publ.) ESA SP, SP-740* (May) (2016) 9–13.
[33] D. Lu, Aboveground biomass estimation using Landsat TM data in the Brazilian Amazon, Int. J. Remote Sens. 26 (12) (2005) 2509–2525, doi:10.1080/01431160500142145.
[34] Dengsheng Lu, M. Batistella, E. Moran, Satellite estimation of aboveground biomass and impacts of forest stand structure, Photogramm. Eng. Remote Sens. 71 (8) (2005) 967–974, doi:10.14358/PERS.71.8.967.
[35] Dengsheng Lu, Q. Chen, G. Wang, L. Liu, G. Li, E. Moran, A survey of remote sensing-based aboveground biomass estimation methods in forest ecosystems, Int. J. Digital Earth 9 (1) (2016) 63–105, doi:10.1080/17538947.2014.990526.
[36] M. Luo, Y. Wang, Y. Xie, L. Zhou, J. Qiao, S. Qiu, Y. Sun, Combination of feature selection and catboost for prediction: the first application to the estimation of aboveground biomass, Forests 12 (2) (2021) 1–22, doi:10.3390/f12020216.
[37] S.D. Madundo, E.W. Mauya, N.J. Lolila, H.A. Mchelu, Modelling and mapping forest above-ground biomass using earth observation data, Int. J. Nat. Resource Ecol. Manag. 7 (1) (2022) 15–21, doi:10.11648/j.ijnrem.20220701.13.
[38] Z. Malenovský, H. Rott, J. Cihlar, M.E. Schaepman, G. García-Santos, R. Fernandes, M. Berger, Sentinels for science: potential of Sentinel-1, -2, and -3 missions for scientific observations of ocean, cryosphere, and land, Remote Sens. Environ. 120 (2012) 91–101, doi:10.1016/j.rse.2011.09.026.
[39] A.M. Masota, M.O. Bollandsås, E. Zahabu, T. Eid, Allometric biomass and volume models for lowland and humid montane forests, in: Allometric Tree Biomass and Volume Models in Tanzania, Department of Forest Resources Assessment, College of Forestry Wildlife and Tourism, Sokoine University of Agriculture, 2016, p. 35.
[40] A.C. Mau, S.C. Reed, T.E. Wood, M.A. Cavaleri, Temperate and tropical forest canopies are already functioning beyond their thermal thresholds for photosynthesis, Forests 9 (1) (2018) 1–24, doi:10.3390/F9010047.
[41] E.W. Mauya, S. Madundo, Above ground biomass and carbon stock of Usambara tropical rainforest in Tanzania, Tanzania J. For. Nat. Conserv. 90 (2) (2021) 63–82.
[42] Ernest William Mauya, S Madundo, Modelling above ground biomass using sentinel 2 and planet scope data in dense tropical montane forests of Tanzania, Tanzania J. For. Nat. Conserv. 91 (1) (2022) 132–153.
[43] G.G. Moisen, T.S. Frescino, Comparing five modelling techniques for predicting forest characteristics, Ecol. Modell. 157 (2–3) (2002) 209–225, doi:10.1016/S0304-3800(02)00197-7.
[44] A.P. Nicolau, A. Flores-Anderson, R. Griffin, K. Herndon, F.J. Meyer, Assessing SAR C-band data to effectively distinguish modified land uses in a heavily disturbed Amazon forest, Int. J. Appl. Earth Obs. Geoinf. 94 (July 2020) (2021) 102214, doi:10.1016/j.jag.2020.102214.
[45] H. Omar, M.A. Misman, A.R. Kassim, Synergetic of PALSAR-2 and sentinel-1A SAR polarimetry for retrieving aboveground biomass in dipterocarp forest of Malaysia, Appl. Sci. (Switzerland) 7 (7) (2017), doi:10.3390/app7070675.
[46] S. Pandit, S. Tsuyuki, T. Dube, Estimating above-ground biomass in sub-tropical buffer zone community forests, Nepal, using Sentinel 2 data, Remote Sens. (Basel) 10 (4) (2018), doi:10.3390/rs10040601.
[47] S. Pandit, S. Tsuyuki, T. Dube, Exploring the inclusion of Sentinel-2 MSI texture metrics in above-ground biomass estimation in the community forest of Nepal, Geocarto Int. 35 (16) (2020) 1832–1849, doi:10.1080/10106049.2019.1588390.
[48] R.L. Pearson, L.D. Milton, Remote mapping of standing crop biomass for estimation of the productivity of the shortgrass prairie, Pawnee National Grasslands, Colorado, in: *Proceedings of the Eighth International Symposium on Remote Sensing of Environment, October, 2–6, 1972*, 1972.
[49] T.D. Pham, N. Yokoya, J. Xia, N.T. Ha, N.N. Le, T.T.T. Nguyen, T.H. Dao, T.T.P. Vu, T.D. Pham, W. Takeuchi, Comparison of machine learning methods for estimating mangrove above-ground biomass using multiple source remote sensing data in the red river delta biosphere reserve, Vietnam, Remote Sens. (Basel) 12 (8) (2020) 1–24, doi:10.3390/RS12081334.
[50] Planet Labs. (2021). *NICFI DATA program - user guide*. 1–12. https://www.planet.com/explorer/
[51] L.G. Poley, G.J. McDermid, A systematic review of the factors influencing the estimation of vegetation aboveground biomass using unmanned aerial systems, Remote Sens. (Basel) 12 (7) (2020), doi:10.3390/rs12071052.
[52] E. Purnamasari, M. Kamal, P. Wicaksono, Comparison of vegetation indices for estimating above-ground mangrove carbon stocks using PlanetScope image, Reg. Stud. Mar. Sci. 44 (2021) 101730, doi:10.1016/j.rsma.2021.101730.
[53] L. Ranghetti, M. Boschetti, F. Nutini, L. Busetto, "sen2r": an R toolbox for automatically downloading and preprocessing Sentinel-2 satellite data, Comput. Geosci. 139 (June) (2020) 104473, doi:10.1016/j.cageo.2020.104473.
[54] F.E. Rex, C.A. Silva, A.P.D. Corte, C. Klauberg, M. Mohan, A. Cardil, V.S. da Silva, D.R.A. de Almeida, M. Garcia, E.N. Broadbent, R. Valbuena, J. Stoddart, T. Merrick, A.T. Hudak, Comparison of statistical modelling approaches for estimating tropical forest aboveground biomass stock and reporting their changes in low-intensity logging areas using multi-temporal LiDAR data, Remote Sens. (Basel) 12 (9) (2020), doi:10.3390/RS12091498.
[55] A.J. Richardson, C.L. Wiegand, Distinguishing vegetation from soil background information, Photogramm. Eng. Remote Sens. 43 (12) (1977) 1541–1552.
[56] J.W. Rouse, R.H. Haas, J.A. Schell, D.W Deering, Monitoring vegetation systems in the great plains with Erts, NASA special publication, in: Proceedings of the Third Earth Resources Technology Satellite- 1 Symposium, 1974, pp. 309–317.
[57] A. Safari, H. Sohrabi, S. Powell, Comparison of satellite-based estimates of aboveground biomass in coppice oak forests using parametric, semiparametric, and nonparametric modeling methods, J. Appl. Remote Sens. 12 (04) (2018) 1, doi:10.1117/1.jrs.12.046026.
[58] M. Shimada, T. Itoh, T. Motooka, M. Watanabe, T. Shiraishi, R. Thapa, R. Lucas, New global forest/non-forest maps from ALOS PALSAR data (2007-2010), Remote Sens. Environ. 155 (2014) 13–31, doi:10.1016/j.rse.2014.04.014.
[59] T. Sivasankar, J.M. Lone, K.K. S, A. Qadir, P.L.N. R, The potential of multi-frequency multipolarized ALOS-2/PALSAR-2 and Sentinel-1 SAR data for aboveground forest biomass estimation, Int. J. Eng. Technol. 10 (3) (2018) 797–802, doi:10.21817/ijet/2018/v10i3/181003095.
[60] J.V. Solórzano, Contrasting the potential of Fourier transformed ordination and gray level co-occurrence matrix textures to model a tropical swamp forest's structural and diversity attributes, J. Appl. Remote Sens. 12 (03) (2018) 1, doi:10.1117/1.jrs.12.036006.
[61] M. Soriano-Luna, Á. de los, G. Ángeles-Pérez, M. Guevara, R. Birdsey, Y. Pan, H. Vaquera-Huerta, J.R. Valdez-Lazalde, K.D. Johnson, R. Vargas, Determinants of above-ground biomass and its spatial variability in a temperate forest managed for timber production, Forests 9 (8) (2018) 1–20, doi:10.3390/f9080490.
[62] A.M.O. Sousa, A.C. Gonçalves, J.R.M. da Silva, Above-ground biomass estimation with high spatial resolution satellite images, in: Biomass Volume Estimation and Valorization for Energy, InTech, 2017, p. 23, doi:10.5772/65665.
[63] H. Tapamo, A. Mfopou, B. Ngonmang, P. Couteron, O. Monga, Linear vs non-linear learning methods A comparative study for forest above ground biomass, estimation from texture analysis of satellite images, Revue Afric. Rech. Inf. Math. Appl. 18 (2014) 114–131, doi:10.46298/arima.1982.
[64] R.B. Thapa, M. Watanabe, T. Motohka, M. Shimada, Potential of high-resolution ALOS–PALSAR mosaic texture for aboveground forest carbon tracking in tropical region, Remote Sens. Environ. 160 (2015) 122–133, doi:10.1016/j.rse.2015.01.007.
[65] K.C. Thumaty, R. Fararoda, S. Middinti, R. Gopalakrishnan, C.S. Jha, V.K. Dadhwal, Estimation of above ground biomass for central Indian deciduous forests using ALOS PALSAR L-band data, J. Indian Soc. Remote Sens. 44 (1) (2016) 31–39, doi:10.1007/s12524-015-0462-4.

[66] M. Urbazaev, C. Thiel, F. Cremer, R. Dubayah, M. Migliavacca, M. Reichstein, C. Schmullius, Estimation of forest aboveground biomass and uncertainties by integration of field measurements, airborne LiDAR, and SAR and optical satellite data in Mexico, Carbon Bal. Manag. 13 (1) (2018), doi:10.1186/s13021-018-0093-5.
[67] E.M. Wood, A.M. Pidgeon, V.C. Radeloff, N.S. Keuler, Image texture as a remotely sensed measure of vegetation structure, Remote Sens. Environ. 121 (2012) 516–526, doi:10.1016/j.rse.2012.01.003.
[68] S. Wood, M.S. Wood, Package "mgcv.", R Package Ver. 1.8-40 1 (29) (2015) 729.